Optical Index Matching, Flexible Electrospun Substrates for Seamless Organic Photocapacitive Sensors

*Timo Grothe, Tobias Böhm, Karim Habashy, Oliya S. Abdullaeva, Jennifer Zablocki, Arne Lützen, Karin Dedek, Manuela Schiek, and Andrea Ehrmann**

Recent advances in optoelectronics are often based on thin-film organic semiconductors. Interesting organic semiconductors are given by squaraines, small molecules that show excitonic coupling with visible light and are thus suitable for applications in solar cells and light sensors. While such squaraine thin films have already been proven to be suitable for stimulation of neuronal model cells, the integration into, e.g., the human eye to support blind people necessitates forming thin layers on seamless substrates. Herein, squaraine films are spin-coated on electrospun nanofiber mats and nanomembranes, prepared from polyacrylonitrile, and made conductive by spin coating with poly(3,4-ethylene-dioxythiophene) polystyrene sulfonate (PEDOT:PSS). The fibrous non-woven texture of the nanofiber mats and membranes alters the thin film formation of the squaraine compound considerably compared with preparation on planar, non-soaking substrates such as glass and polyethylene terephthalate (PET) foil demanding further engineering regarding material's choice and processing conditions.

T. Grothe, T. Böhm, Prof. A. Ehrmann
Institute for Technical Energy Systems (ITES)
Bielefeld University of Applied Sciences
33619 Bielefeld, Germany
E-mail: andrea.ehrmann@fh-bielefeld.de

K. Habashy, Dr. O. S. Abdullaeva, Prof. M. Schiek,[+]
Institute of Physics
University of Oldenburg
Carl-von-Ossietzky-Straße 9–11, 26129 Oldenburg, Germany

J. Zablocki, Prof. A. Lützen
Kekulé Institute of Organic Chemistry and Biochemistry
University of Bonn
Gerhard-Domagk-Str. 1, 53121 Bonn, Germany

Prof. K. Dedek
Neurosensorics/Animal Navigation
Institute for Biology and Environmental Sciences
University of Oldenburg
Carl-von-Ossietzky-Straße 9–11, 26129 Oldenburg, Germany

The ORCID identification number(s) for the author(s) of this article can be found under https://doi.org/10.1002/pssb.202000543.

[+]Present address: LIOS & ZONA, Johannes Kepler University, Altenberger Str. 69, A-4040 Linz, Austria

1. Introduction

One of the emerging areas in bioelectronic medical implants is the development of retinal prostheses, using self-powered photovoltaic devices to convert optical signals into electric stimuli.[1,2] While the rigidity of silicon-based devices is a challenge for their implantation into the eyeball, organic semiconductors could be coated on flexible and drapable substrates which would allow for fitting them exactly to the shape and the mechanical properties of the human retina.[3,4] For this, diverse approaches have been tested by different research groups, including carbon nanotubes, graphene and graphene–polymer hybrids,[5–7] polymers,[8–10] and organic small molecules.[11–14]

Among the latter squaraines are promising compounds that, due to their strong excitonic interaction with visible light combined with semiconducting properties,[15–17] have been widely implemented into photovoltaic light harvesting[18–20] and sensing[21–24] devices and subjected to fundamental molecular excitonic studies.[25–29] Especially appealing are the environmental robustness and the polymorphic structural variety[30,31] that merge into a functional self-patterning of microcrystalline thin films.[32] To eventually allow for in vivo operation of such optoelectronic device, fabrication on a biocompatible substrate is necessary.

Such a substrate must be flexible and ideally also drapable to be fitted to the retina, both parameters that can typically be found in many textile fabrics. While macroscopic textiles are naturally not suitable for this application, electrospun nanofiber mats and nanomembranes are possible candidates as low-cost alternative to spider silk.[33,34] Electrospinning is a primary spinning technique which can be used to prepare continuous nanofibers or nanofiber mats with typical fiber diameters in the range of some ten to several hundred nanometers.[35–37] Their large specific surface makes them well-suited for diverse applications such as filters, catalysts, bioengineering, tissue engineering, and wearables.[38–41] For in vivo applications, it is reasonable to use nontoxic or low-toxic solvents for processing, such as dimethyl sulfoxide (DMSO), and polymers which can be dissolved in it.[42] An ideal candidate is polyacrylonitrile (PAN), being unambiguously spinnable from DMSO and not showing cell toxicity.[43,44] As intended, PAN nanofiber mats can be stretched and draped in a wet state.[45] As additional

benefit, the PAN nanofiber mats, which appear white due to light scattering in the dry state, become transparent when soaked with liquid[46] due to refractive index matching.[47] For conductivity purposes, the nanofiber mats are further coated with poly(3,4-ethylenedioxythiophene) polystyrene sulfonate (PEDOT:PSS), a polymer-based electrode material commonly used in the field of bioelectronics.[48–50]

Here, we report on a first study investigating PAN nanofiber mats and nanomembranes as seamless, biocompatible substrate alternative to the previously used glass substrates for squaraine-based neurostimulating photocapacitpors[12,14] assessing morphology, structure, and optical properties of the photoactive layer.

2. Results and Discussion

Three types of PAN substrates have been fabricated differing in their texture. While the mats are rather loosely spun retaining the electrospun nanofibers as a mesh, the nanofibers join up with increasing degree of coalescence for the mat-membranes and membranes. However, all three types are substantially rougher and even soaking compared with indium tin oxide (ITO)-covered glass or polyethylene terephthalate (PET) substrates. The latter typically have surface roughnesses of a few nanometers, while the surface roughness for PAN substrates is in the range of the nanofiber diameter, i.e., of few hundred nanometers. In a first step, the PAN substrates were coated with PEDOT:PSS to install conductivity, which is essential for the photocapacitive sensor performance.[12,14] The PEDOT:PSS is basically soaked up by all PAN samples resulting in a sheet resistance of (500 ± 100) Ω. This is still a factor of three lower than what is required to perform as stand-alone electrode in a polymer photovoltaic cell.[53] For comparison, the sheet resistances of the ITO-covered glass and

PET foil have been determined to be (8 ± 2) Ω and (55 ± 5) Ω (60 Ω nominal value by company), respectively.

The coarse texture of the PEDOT:PSS-coated PAN substrates clearly affects the thin film formation of spincasted and thermally annealed 2,4-bis[4-(N,N-diisobutylamino)-2,6-dihydroxyphenyl] squaraine (SQIB) layers compared with nonpermeable substrates (see **Figure 1**). A weakly bireflectant, fine-grained and discontinuous layer can be seen in an optical microscope between crossed polarizers on the PAN substrates (Figure 1a–c). The crystallite size appears to increase from mat over mat-membrane to membrane spotted by areas of increased golden or bright green bireflectance. On the contrary, a few hundreds of micrometer wide, strongly bireflectant golden SQIB platelets can be seen on ITO glass and ITO–PET (Figure 1d,e), respectively. They cover the surface almost completely. From previous studies we know that these platelets are made up of the orthorhombic SQIB polymorph[12,14,30] in the present case with a bottom layer of PCBM, which phase separates during the thermal annealing step.[14,32] Thereby, the presence of PCBM essentially does not disturb the crystallization and texture of SQIB, so that this blended coatings can be used for comparison purposes regarding the thin film formation. X-ray diffraction (XRD) indicates the presence of both known SQIB polymorphs with a slightly varying share of the orthorhombic polymorph (Figure 1f). Note the XRD scattering cross section of the monoclinic polymorph is smaller;[30] therefore, the diffraction peak ratio does not allow a conclusion on the proportion of monoclinic and orthorhombic polymorph. Interesting to note that only a single out-of-plane orientation, i.e., (110) for the orthorhombic and (011) for the monoclinic polymorph, is realized, just as it is the case for rigid substrates.[10,14,30,32] As the XRD signals overall are weak, we assume the major fraction of SQIB to be in an amorphous state. This is in accordance with the faint mossy-green
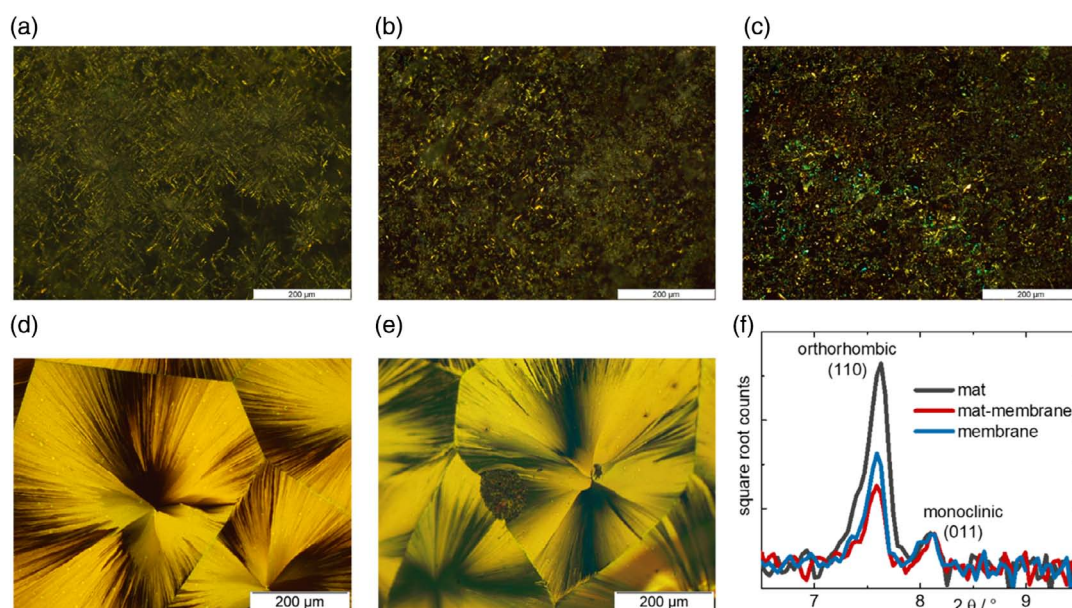

Figure 1. Optical microscopy images between crossed polarizers of a) nanofiber mats, b) mat-membranes, and c) membranes after coating with PEDOT:PSS and SQIB and thermal annealing at 180 °C. Scale bars are 200 µm. d,e) A spin-coated SQIB:PCBM (3:1) blend on ITO-covered glass and ITO-covered PET, respectively, after thermal annealing at 180 °C is shown. f) XRD patterns of the samples imaged in the upper row are plotted.
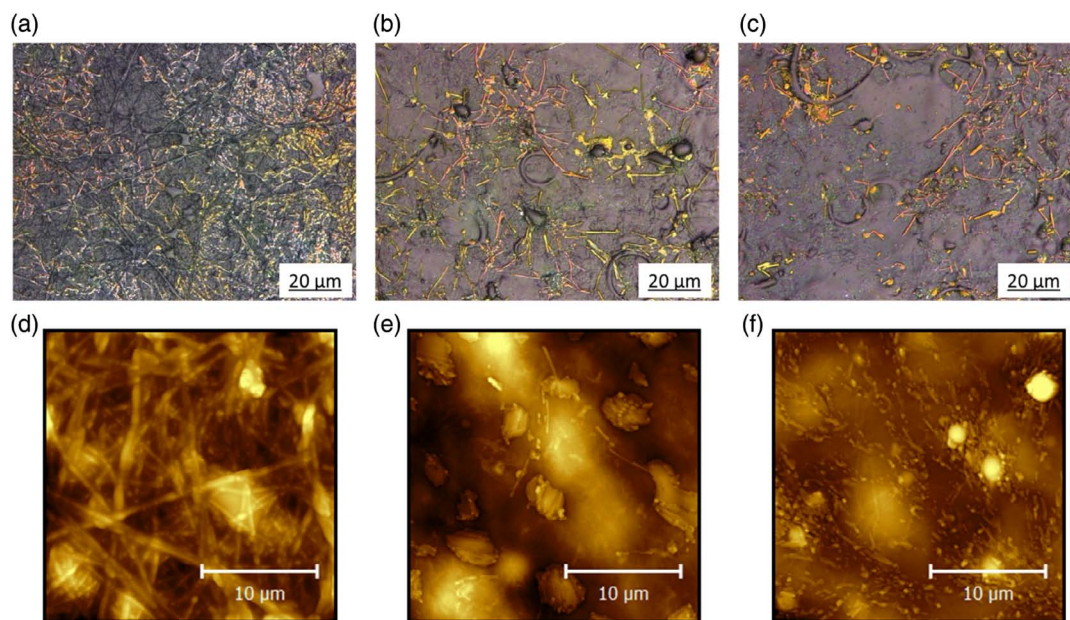
Figure 2. Upper row: CLSM images, lower row: intermittant contact mode AFM images of a,d) nanofiber-mats, b,e) mat-membranes, and c,f) membranes subsequently spin-coated with PEDOT:PSS and SQIB followed by thermal annealing at 180 °C.

background color of the microscopy images, as shown in Figure 1a–c.

The morphology of the samples is further investigated by confocal laser scanning microscope (CLSM) (**Figure 2**a–c) and atomic force microscope (AFM) (Figure 2d–f). For the PAN mat substrates (Figure 2a,d), the nonwoven texture of the electrospun PAN nanofibers dominates the morphology impression of the samples. On the mat-membranes (Figure 2b) and membranes (Figure 2c), CLSM resolves brown-golden nanorods on the surface, which most likely consist of the SQIB orthorhombic polymorph.[30] Clearly, the SQIB coating is highly discontinuous, contrasting the cohesive layer formation on rigid, nonsoaking substrates. However, this must not necessarily be a hindrance for the functionality as a photocapacitor for neurostimulation targeting a spatial resolution on single-cell scale. Indeed, this discontinuity reinforces the spatial self-patterning capability into functional sub-microscaled units.[32]

Next, transmission and reflection properties were investigated for all three coated PAN substrates. We have already shown that electrospun membranes are translucent, while nanofiber mats appear white in the dry state due to scattering. Upon soaking with water such nanofiber mats become almost transparent.[46] Here, the PAN substrates have been coated with a water-soluble PEDOT:PSS formulation, which unfortunately does not tolerate immersion experiments in water. For future experiments, we will install water stability by adding cross-linking agents to the PEDOT: PSS formulation.[9,34] The total transmission and total reflection spectra (where total refers to scattering included) of PAN substrates already covered with PEDOT:PSS are shown in **Figure 3**a, dark gray curves. The nanofiber mat shows the lowest transmission and the highest reflection, which can be attributed to more PEDOT:PSS soaked into the substrate, and scattering from the nanofibrous texture. Transmission increases while

reflection decreases for the progressively more close-meshed mat-membranes (red curves) and membranes (blue curves).

After SQIB coating on either substrate or thermal annealing, the typical SQIB absorption causes a broad transmission dip from 550 to 750 nm (Figure 3b). This dip clearly is largest for the mat (dark gray curve), indicating that this rather loosely nonwoven nanofiber mat has the largest capacity to soak up SQIB material. From this broad absorbance alone on a rough substrate, it cannot be judged if SQIB is in an amorphous phase or crystalized or a mixture of both. For comparison, the total transmission spectra of a SQIB:PCBM (3:1 wt%) blend spin-coated on ITO-covered glass or PET foil are shown in Figure 3c. Thermal annealing at 180 °C results in basically the same absorption features (green and golden curves) dipping at 655 and 735 nm for SQIB on either substrate, indicating the well-characterized Davydov splitting of the orthorhombic polymorph.[30,32] This is in line with polarized optical microscopy inspection, as shown in Figure 2d,e. In addition, the absorption of the PCBM can be noted at wavelengths below 400 nm. However, the substrates become opaque at wavelength below 350 nm, which should not be confused with photoactive layer absorption. Annealing at 60 °C does not induce crystallization, yet results in a similarly broad transmission dip but with only one pronounced minimum at 690 nm including a vibronic shoulder at shorter wavelength.[30]

Interestingly, the reflection is strongly reduced over the whole wavelength range under examination for all coated PAN substrates (Figure 3b, dotted curves). This suggests that SQIB effectively acts as interspace-filler suppressing the scattering potential of the samples, effectively reducing possible scattering losses of the anticipated photocapacitor device.[54] Likely, the interspace-wetting is enforced by the thermal annealing step.[55]
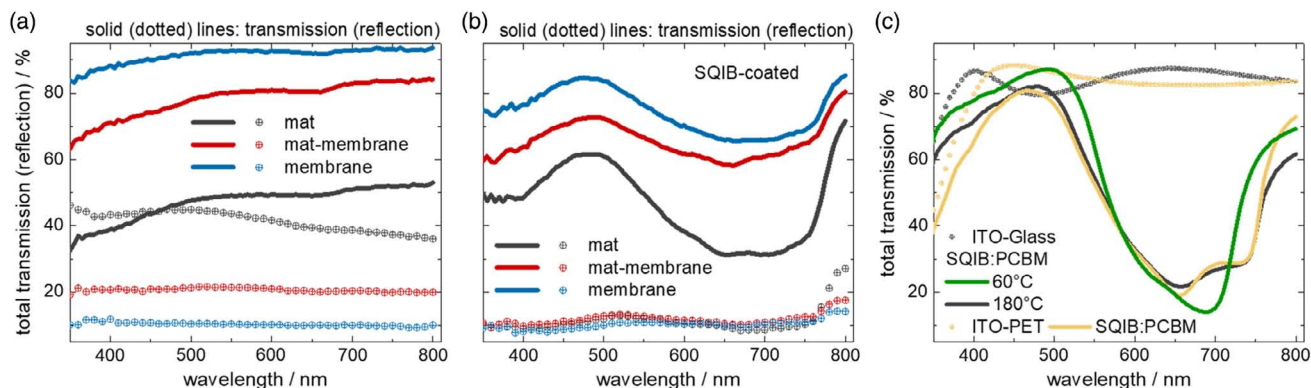
Figure 3. a) Total transmission (straight lines) and total reflection (dots) of PEDOT:PSS covered nanofiber mats (dark grey), mat-membranes (red), and membranes (blue). b) Total transmission (straight lines) and total reflection (dots) of the same PAN substrates as in (a) but additionally spin-coated with SQIB followed by thermal annealing at 180 °C. c) Total transmission of ITO-covered glass (dark-gray dots) and PET foil (golden dots) and these substrates spin-coated with a SQIB:PCBM blend subsequently annealed at 60 °C (green line, on ITO glass), at 180 °C on ITO glass (dark grey line) and ITO–PET (golden line). PCBM contributes to the photoactive layer absorption at wavelength below 400 nm.

3. Conclusion

We have approached photocapacitive sensor targeted for in vivo stimulation of neuronal cells on drapable substrates consisting of more or less densely arranged electrospun PAN nanofiber mats. These nonwoven substrates could successfully be made conductive with a PEDOT:PSS coating. Due to the permeable nature of the PAN substrates, the thin film formation of a spin-coated and thermally annealed squaraine is significantly altered compared with nonsoaking substrates such as ITO-covered glass or PET foil. However, the absorption capability is reasonable, and the very low surface reflection clearly is promising to decrease reflection losses for device operation. As soon as the water solubility of the PEDOT:PSS layer is overcome, the PAN mats will reveal their invincible benefit, in addition to mechanical flexibility, of becoming seamless due to transparency in wet environment.

4. Experimental Section

Substrates were prepared using the wire-based electrospinning machine "Nanospider Lab" (Elmarco Ltd., Liberec, Czech Republic), applying the following spinning parameters: voltage 70 kV, nozzle diameter 0.8–1.5 mm, carriage speed 100 mm s^{-1}, bottom electrode/substrate distance 240 mm/120 mm, ground electrode/substrate distance 50 mm, temperature in the chamber 22–23 °C, and relative humidity in the chamber 31%–32%. The bottom electrode/substrate distance enables defining the membrane structure: while the largest distance results in pure nanofibers, the smallest distance enables electrospinning closed membranes without fibrous structure.[51] Substrates were prepared by electrospinning for 20 min at the maximum distance ("nanofiber mat" or "mats"), for 20 min at the minimum distance ("membrane"), or for 10 min each at the maximum and the minimum distance to combine the closed area of the nanomembrane with the good mechanical properties of the nanofiber mat ("mat-membrane"). The substrates were mounted on 15 × 15 mm^2 cover slips for the following spin-coating procedure.

Spinning solutions contained 14% PAN (X-PAN, Dralon, Dormagen, Germany) dissolved in DMSO (minimum 99.9%, purchased from S3 Chemicals, Bad Oeynhausen, Germany) by 2 h stirring on a magnetic stirrer, followed by resting for 1 day.

The substrates were subsequently coated with PEDOT:PSS (Orgacon S305) and SQIB.[12,30] Spincoating of PEDOT:PSS was conducted in ambient conditions (Laurell WS 400). The substrates were transferred into a nitrogen-filled glove box and dried at 100 °C for 20 min on a hotplate (IKA yellowline). A 6 mg mL^{-1} SQIB solution in amylene-stabilized chloroform (Sigma-Aldrich) was then spin-coated (SÜSS MicroTec LabSpin) at 3000 rpm followed by thermal annealing at 180 °C for 60 min. For comparison purposes, ITO-covered glass (Temicon) and PET foil (Sigma-Aldrich) were spin-coated with a mixture of SQIB and phenyl-C61-butyric acid methyl ester (PCBM, Solenne) (3:1 wt%, 8 mg mL^{-1} total concentration in chloroform) followed by thermal annealing at 180 °C for 60 min.

Morphological investigations of the coated surfaces were performed by a CLSM VK-8710 (Keyence, Neu-Isenburg, Germany) and by an AFM FlexAFM Axiom (Nanosurf, Liestal, Switzerland) in tapping mode, using a Tap190Al-G-10 tip. Polarized optical microscopy images have been recorded using an Olympus BX41 optical microscope equipped with crossed polarizers.

Sheet resistance has been determined via van der Pauw method using standard procedure and correction function.[52] For this, the samples were contacted with probe pads in four corners, and I–V curves have been recorded with a Keithley 2400 source measure unit.

Total transmission and reflection were recorded with a Bentham PVE300 system equipped with a Czerny-Turner TMc300 monochromator and an integrating sphere using a Xenon lamp as light source (8° angle of incidence). The monochromator slit was set to 1.85 mm, and the light beam was formed with a quadratic mask to 1.85 × 1.85 mm^2.

XRD was performed in Bragg–Brentano geometry in a PANalytical X'PertPro MPD diffractometer using Cu Kα radiation ($\lambda = 1.542$ Å) at 40 kV and 40 mA, using a 10 mm beam mask. Samples were rotated in a sample spinner during scanning to average over in-plane orientations.

Conflict of Interest

The authors declare no conflict of interest.

Data Availability Statement

The data that support the findings of this study are available from the corresponding author upon reasonable request.

[1] D. Palanker, G. Goetz, *Phys. Today* **2018**, *71*, 26.
[2] L. N. Ayton, N. Barnes, G. Dagnelie, T. Fujikado, G. Goetz, R. Horning, B. W. Jones, M. M. K. Muqit, D. L. Rathbun, K. Stingl, J. D. Weiland, M. A. Petoe, *Clin. Neurophysiol.* **2020**, *131*, 1383.
[3] G. J. Lee, C. Choi, D.-H. Kim, Y. M. Song, *Adv. Funct. Mater.* **2018**, *28*, 1705202.
[4] L. Ferlauto, M. J. I. A. Leccardi, N. A. L. Chenais, S. C. A. Gilliéron, P. Vagni, M. Bevilacqua, T. J. Wolfensberger, K. Sivula, D. Ghezzi, *Nat. Commun.* **2018**, *9*, 992.
[5] L. Bareket, N. Waiskopf, D. Rand, G. Lubin, M. David-Pur, J. Ben-Dov, S. Roy, C. Eleftheriou, E. Sernagor, O. Cheshnovsky, U. Banin, Y. Hanein, *Nano Lett.* **2014**, *14*, 6685.
[6] A. Savchenko, V. Cherkas, C. Liu, G. B. Braun, A. Kleschevnikov, Y. I. Miller, E. Molokanova, *Sci. Adv.* **2018**, *4*, eaat0351.
[7] M. L. Di Francesco, E. Colombo, E. D. Papaleo, J. F. Maya-Ventencourt, G. Manfredi, G. Lanzani, F. Benfenati, *Carbon* **2020**, *162*, 308.
[8] D. Ghezzi, A. R. Antognazza, R. Maccarone, S. Bellani, E. Lanzarini, N. Marino, M. Mete, G. Pertile, S. Bisti, G. Lanzani, F. Benfenati, *Nat. Photon.* **2013**, *7*, 400.
[9] M. Han, S. B. Srivastava, E. Yildiz, R. Melikov, S. Surme, I. B. Dogru-Yuksel, I. H. Kavakli, A. Sahin, S. Nizamoglu, *ACS Appl. Mater. Interfaces* **2020**, *12*, 38.
[10] M. J. I. A. Leccardi, N. A. L. Chenais, L. Ferlauto, M. Kawecki, E. G. Zollinger, D. Ghezzi, *Commun. Mater.* **2020**, *1*, 21.
[11] M. Sytnyk, M. Jakesova, M. Litvinukova, O. Mashkov, D. Kriegner, J. Stangl, J. Nebesarova, F. W. Fecher, W. Schöfberger, N. S. Sariciftci, R. Schindl, W. Heiss, E. D. Głowacki, *Nat. Commun.* **2017**, *8*, 91.
[12] O. S. Abdullaeva, M. Schulz, F. Balzer, J. Parisi, A. Lützen, K. Dedek, M. Schiek, *Langmuir* **2016**, *32*, 8533.
[13] D. Rand, M. Jakesova, G. Lubin, I. Vebraite, M. David-Pur, V. Derek, T. Cramer, N. S. Sariciftci, Y. Hanein, E. D. Głowacki, *Adv. Mater.* **2018**, *30*, 1707292.
[14] O. S. Abdullaeva, F. Balzer, M. Schulz, J. Parisi, A. Lützen, K. Dedek, M. Schiek, *Adv. Funct. Mater.* **2019**, *29*, 1805177.
[15] S. Sreejith, P. Carol, P. Chithra, A. Ajayaghosh, *J. Mater. Chem.* **2008**, *18*, 264.
[16] K. Ilina, W. M. MacCuaig, M. Laramie, J. N. Jeouty, L. R. McNally, M. Henary, *Bioconjug. Chem.* **2020**, *31*, 194.
[17] G. M. Xia, H. M. Wang, *J. Photochem. Photobiol. C* **2017**, *31*, 84.
[18] Y. Chen, W. Zhu, J. Wu, Y. Huang, A. Facchetti, T. J. Marks, *Org. Photonics Photovolt.* **2019**, *7*, 1.
[19] G. Chen, Z. Ling, B. Wie, J. Zhang, Z. Hong, H. Sasabe, J. Kido, *Front. Chem.* **2018**, *6*, 412.
[20] D. Scheunemann, O. Kolloge, S. Wilken, M. Mack, J. Parisi, M. Schulz, A. Lützen, M. Schiek, *Appl. Phys. Lett.* **2017**, *111*, 183502.
[21] P. Salice, E. Ronchi, A. Iacchetti, M. Binda, D. Natali, W. Gomulya, M. Manca, M. A. Loi, M. Iurlo, F. Paolucci, M. Maggini, G. A. Pagani, L. Beverina, E. Menna, *J. Mater. Chem. C* **2014**, *2*, 1396.
[22] M. Schulz, M. Mack, O. Kolloge, A. Lützen, M. Schiek, *Phys. Chem. Chem. Phys.* **2017**, *19*, 6996.
[23] K. Strassel, A. Kaiser, S. Jenatsch, A. C. Véron, S. B. Anantharaman, E. Hack, M. Diethelm, F. Nüesch, R. Aderne, C. Legnani, S. Yakunin, M. Cremona, R. Hany, *ACS Appl. Mater. Interfaces* **2018**, *10*, 11063.
[24] M. Schulz, F. Balzer, D. Scheunemann, O. Arteaga, A. Lützen, S. C. J. Meskers, M. Schiek, *Adv. Funct. Mater.* **2019**, *29*, 1900684.
[25] C. Zhong, D. Bialas, C. J. Collison, F. C. Spano, *J. Phys. Chem. C* **2019**, *123*, 18734.
[26] M. I. S. Röhr, H. Marciniak, J. Hoche, M. H. Schreck, H. Ceymann, R. Mitric, C. Lambert, *J. Phys. Chem. C* **2018**, *122*, 8082.
[27] N. Auerhammer, A. Schmiedel, M. Holzapfel, C. Lambert, *J. Phys. Chem. C* **2018**, *122*, 11720.
[28] P. Malý, J. Lüttig, A. Turkin, J. Dostál, C. Lambert, T. Brixner, *Chem. Sci.* **2020**, *11*, 456.
[29] M. Schulz, J. Zablocki, O. S. Abdullaeva, S. Brück, F. Balzer, A. Lützen, O. Arteaga, M. Schiek, *Nat. Commun.* **2018**, *9*, 2413.
[30] F. Balzer, H. Kollmann, M. Schulz, G. Schnakenburg, A. Lützen, M. Schmidtmann, C. Lienau, M. Silies, M. Schiek, *Crystal Growth Design* **2017**, *17*, 6455.
[31] J. Zablocki, O. Arteaga, F. Balzer, D. Hertel, J. J. Holstein, G. Clever, J. Anhäuser, R. Puttreddy, K. Risannen, K. Meerholz, A. Lützen, M. Schiek, *Chirality* **2020**, *32*, 619.
[32] F. Balzer, O. S. Abdullaeva, A. Maderitsch, M. Schulz, A. Lützen, M. Schiek, *Phys. Status Solidi B* **2020**, *257*, 1900570.
[33] C. Holland, K. Numata, J. Rnjak-Kovacina, P. Seib, *Adv. Healthcare Mater.* **2019**, *8*, 1800465.
[34] J. F. Maya-Vetencourt, D. Ghezzi, M. R. Antognazza, E. Colombo, M. Mete, P. Feyen, A. Desii, A. Buschiazzo, M. D. Paolo, S. D. Marco, F. Ticconi, L. Emionite, D. Shmal, C. Marini, I. Donelli, G. Freddi, R. Maccarone, S. Bisti, G. Sambuceti, G. Pertile, G. Lanzani, F. Benfenati, *Nat. Mater.* **2017**, *16*, 681.
[35] D. Li, Y. Xia, *Adv. Mater.* **2004**, *16*, 1151.
[36] S. Agarwal, A. Greiner, J. H. Wendorff, *Prog. Polym. Sci.* **2013**, *38*, 963.
[37] T. Grothe, J. L. Storck, M. Dotter, A. Ehrmann, *Tekstilec* **2020**, *63*, 225.
[38] R. Roche, F. Yalcinkaya, *Chem. Open* **2019**, *8*, 97.
[39] L. Kumar, S. Singh, A. Horechyy, P. Formanek, R. Hübner, V. Albrecht, J. Weißpflog, S. Schwarz, P. Puneet, B. Nandan, *RSC Adv.* **2020**, *10*, 6592.
[40] C. Großerhode, D. Wehlage, T. Grothe, N. Grimmelsmann, S. Fuchs, J. Hartmann, P. Mazur, V. Reschke, H. Siemens, A. Rattenholl, S. V. Homburg, A. Ehrmann, *AIMS Bioeng.* **2017**, *4*, 376.
[41] J. Xiong, J. Chen, P. S. Lee, *Adv. Mater.* **2020**, 202002640.
[42] M. Wortmann, N. Frese, L. Sabantina, R. Petkau, F. Kinzel, A. Gölzhäuser, E. Moritzer, B. Hüsgen, A. Ehrmann, *Nanomaterials* **2019**, *9*, 52.
[43] D. Wehlage, H. Blattner, L. Sabantina, R. Böttjer, T. Grothe, A. Rattenholl, F. Gudermann, D. Lütkemeyer, A. Ehrmann, *Tekstilec* **2019**, *62*, 78.
[44] D. Wehlage, H. Blattner, A. Mamun, I. Kutzli, E. Diestelhorst, A. Rattenholl, F. Gudermann, D. Lütkemeyer, A. Ehrmann, *AIMS Bioeng.* **2020**, *7*, 43.
[45] T. Grothe, L. Sabantina, M. Klöcker, I. J. Junger, C. Döpke, A. Ehrmann, *Technologies* **2019**, *7*, 23.
[46] E. Kerker, D. Steinhäußer, A. Mamun, M. Trabelsi, J. Fiedler, L. Sabantina, I. J. Junger, M. Schiek, A. Ehrmann, R. Kaschuba, *Optik* **2020**, *208*, 164081.

[47] G. Jacucci, L. Schwertel, Y. Zhang, H. Yang, S. Vignolini, *Adv. Mater.* **2020**, 202001215.

[48] X. Fan, W. Nie, H. Tsai, N. Wang, H. Huang, Y. Cheng, R. Wen, L. Ma, F. Yan, Y. Xia, *Adv. Sci.* **2020**, *6*, 190081.

[49] J. Rivnay, S. Inal, B. A. Collins, M. Sessolo, E. Stravrinidou, X. Strakosas, C. Tassone, D. M. Delongchamp, G. G. Malliares, *Nat. Commun.* **2016**, *7*, 11287.

[50] R. Samba, T. Herrmann, G. Zeck, *J. Neural Eng.* **2015**, *12*, 016014.

[51] L. Sabantina, L. Hes, J. Rodríguez-Mirasol, T. Cordero, A. Ehrmann, *Fibres Text. East. Eur.* **2019**, *133*, 12.

[52] A. A. Ramadan, R. D. Gould, A. Ashour, *Thin Solid Films* **1994**, *239*, 272.

[53] F. Zhang, M. Johansson, M. R. Andersson, J. C. Hummelen, O. Inganäs. *Adv. Mater.* **2002**, *14*, 662.

[54] J. Cai, L. Qi, *Mater. Horiz.* **2015**, *2*, 37.

[55] K. Bordo, M. Schiek, A. Ghazal, I. Wallmann, A. Lützen, F. Balzer, H.-G. Rubahn, *J. Phys. Chem. C* **2011**, *115*, 20882.